Indian Journal of Chemical Technology
Vol. 32, March 2025, pp. 290-302
DOI: 10.56042/ijct.v32i2.5327

A quantum chemical and experimental study on the protective performance of N-(4-(piperidin-1-ylsulfonyl)phenyl)acetamide for mild steel corrosion

K. Vijayalakshmi* & J. Elangovan*

PG and Research Department of Chemistry, Rajah Serfoji Government College (A) (Affiliated to Bharathidasan University, Tiruchirappalli), Thanjavur-613 005, Tamil Nadu, India

*E-mail: vijikraja96@gmail.com (KV); elangoorganic@gmail.com (JE)

Received 3 September 2023; accepted 3 February 2025

In this study, the anticorrosive potential of N-(4-(piperidin-1-ylsulfonyl)phenyl)acetamide (PSPA) in the 1M HCl solution has been investigated. An inhibitory efficiency of 96% at 30 ppm is achieved using the polarization, mass reduction, and impedance approaches. To pinpoint the precise modes of the adsorption process, the kinetic, thermodynamic, and adsorption parameters are studied at various temperatures. The protective probability of the examined inhibitor is further evaluated by employing Density Functional Theory. Additional crucial information on the inhibitory mechanism is provided by the Fukui condensed function. Conclusively, various parameters are used to confirm the protective properties of the thin film, including SEM, EDS, and AFM.

Keywords: Corrosion, Density Functional Theory, Fukui function, Inhibitory mechanism, Mild steel, Thermodynamic

Introduction

Due to their appealing properties, metals, and related alloys are widely used resources that are primarily responsible for the socio-economic enhancement and growth of numerous fields[1,2]. Nevertheless, the economy and public safety have been seriously jeopardized by metallic corrosion brought on by the harsh environment. As a result, multiple industries are thus suffering enormous losses of revenue[3]. Hence, Corrosion prevention is essential to alleviating the financial strain and persistent issues caused by corrosion, which is a pervasive and expensive ecological concern on a global scale. Therefore, several efforts have been made to lessen the disintegration of metal and metal alloys under acidic conditions[4]. Hence heterocyclic candidates have been employed in this context because of their superior inhibitory effects brought on by their molecular structures, low consumption of toxic substances, and the capacity to form protective layers against corrosion[5,6].

Theoretically, the efficacy of the inhibitors is given by their interaction with metals, and DFT is the key technique for understanding this. The major sources of this illustration are Highest Occupied Molecular Orbital Energies (E_{HOMO}) and Lowest Unoccupied Molecular Orbital Energies (E_{LUMO}), which are extracted from the optimized stricture of the investigated inhibitors. To determine the reactivity and the inhibitor-Mild steel interactions, additional essential electronic properties from the Frontier Molecular Orbitals (FMO) are also acquired, including the energy gap (ΔE), ionization energy (I), absolute electronegativity (χ), electron affinity (A), global hardness (η), global softness (σ), the fraction of electron transferred (N), and back donation ($E_{Backdonation}$)[7,8]. Application of the Fukui condensed function to identify the electrophilic and nucleophilic locations of the inhibitor advances our understanding of corrosion inhibition [9,10].

Numerous heterocyclic compounds have gained recognition in recent years as potent anti-corrosive agents. These include piperidine derivatives, and certain subsets of these piperidine derivatives are efficacious corrosion inhibitors, particularly in the 1M HCl medium[11–13]. Although heterocyclic compounds are well-established for their corrosion inhibition properties, derivatives of piperidine have not been extensively investigated. Consequently, in this context, we have examined the anticorrosive potential of N-(4-(piperidin-1-ylsulfonyl)phenyl)acetamide (PSPA) in 1M HCl utilizing a combination of polarization, gravimetric, and impedance techniques. The deliberate incorporation of both piperidine and sulfonyl groups in PSPA is noteworthy. The nitrogen atoms in the piperidine ring can enhance adhesion to

metal surfaces, while sulfonyl groups are recognized for their capacity to increase solubility and adsorption efficiency. This combination is hypothesized to produce a synergistic effect, enhancing overall corrosion inhibition performance. Furthermore, the utilization of IRSM 41-97 steel in this research is significant. This versatile material exhibits a combination of high strength, superior corrosion resistance, and aesthetic appeal. Its distinctive properties render it a preferred choice across various sectors, including railway infrastructure, maritime applications, construction, and industrial equipment manufacturing. The selection of IRSM 41-97 steel may potentially confer benefits such as reduced maintenance costs, extended service life, and improved performance in adverse environmental conditions.

This investigation elucidates the unique inhibitory properties of PSPA when utilized in low concentrations. The experimental findings demonstrated that PSPA attained an inhibition efficiency of 96% at a concentration of 30 ppm. Furthermore, quantum chemical analyses, encompassing Density Functional Theory (DFT) and Fukui function evaluations, in conjunction with morphological examinations, substantiate the robust anti-corrosion efficacy of PSPA under acidic conditions.

Experimental Section

Materials

For the preparation of inhibitors, analytical-grade solvents and reagents were employed. The chemicals such as 37% HCl, chlorosulfonic acid, acetanilide, carbon tetrachloride, dichloromethane, piperidine, and ethanol were purchased from Techno Scientific in India.

Specimen preparation

The specimens utilized in this study were commercially available IRSM41/97 grade Mild steel. The elemental analysis of Mild steel specimens studied indicated: "Fe 99.69%, C - 0.076 %, S - 0.009 %, P - 0.08 %, Cu - 0.31%, Ni - 0.20%, Mn - 0.43%, Cr - 0.52%, Si - 0.319% and Al - 0.028%". The specimens used were rectangular-shaped pieces of mild steel with the following measurements: “5cm X 2 cm X 0.2 cm”. A wide range of stainless steel specimens were prepared by polishing each one with silicon carbide sheets. The polished specimens were cleaned with distilled water, ethanol, and acetone after they had been cleaned with silicon carbide sheets (200, 400, 600, 800, 1200, and 1500 grades). In this experiment, 1.0 M HCl was used as the corrosive medium.

Synthesis of PSPA

Under cold conditions, acetanilide (3 g, 21.87 mmol) was added with chlorosulfonic acid (13 mL, 61.61 mmol) drop by drop. The mixture was then stirred for three hours. The mixture from the reaction was poured into the broken ice when it had finished, and carbon tetrachloride was used to extract it. After washing the mixed organic layers with the dilute sodium carbonate solution, 4-acetamido benzene sulfonyl chloride was procured by solvent evaporation[14,] Afterward, the above-obtained product (1.5 g, 6.41 mmol) and piperidine (7.0 mL, 9.63 mmol) in dichloromethane were stirred for 30 minutes at room temperature yielded N-(4-(piperidin-1-ylsulfonyl) phenyl) acetamide. The synthesized inhibitor (PSPA) was rinsed with water, filtered, and dried [15]. Table 1 provides the molecular structure and analytical information for the protector.

Mass loss method

A new batch of mild steel samples was prepared for the mass loss method and then weighed accurately before and after immersion in 1M HCl corrosion solution for 6 h at room temperature in different concentrations of PSPA. A corrosion test was conducted on the specimens after they had been

Table 1 — Analytical information for PSPA

Name	Structure	Analytical data
N-(4-(piperidin-1-ylsulfonyl) phenyl) acetamide	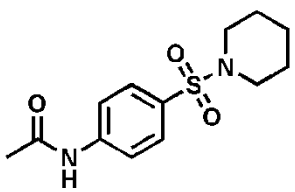	**Appearance:** Milky white solid **Melting Point:** 108-110^{o}C **“^{1}H NMR (500 MHz, $CDCl_3$, δ (ppm)):** 7.70 (*d, J* = 8, 2H), 7.39 (s, 1H), 7.33-7.25 (*m*, 3H), 7.16 (*d, J*=4, 2H), 6.95 (*d, J* = 8, 2H), 4.64 (*t, J* = 8, 2H), 3.84 (s, 3H), 3.26 (*t, J* = 8, 2H)” **“^{13}C NMR (125 MHz, $CDCl_3$, δ (ppm)):** 159.6, 147.4, 137.1, 128.8, 128.7, 127.1, 127.0, 123.4, 119.2, 114.2, 55.3, 51.7”

cleaned, dried, and accurately weighed. Three successive mass loss investigations were conducted under the same settings, and the average weight loss was obtained for this evaluation[16,17]. As part of our study, we used Eqs (1), (2), and (3) to determine the corrosion variables, such as the rate of corrosion (CR), inhibition efficiency (IE), and surface coverage (θ).

$$CR = \frac{\Delta W}{At} \quad \ldots (1)$$

$$I.E(\%) = \left(\frac{W_0 - W}{W_0}\right) \times 100 \quad \ldots (2)$$

This formula contains "ΔW" as the average mass loss (mg), "A "as the total surface area (cm^{-2}), and "t" as the exposure time (h) when testing specimens in 1M HCl with and without inhibitor.

$$\theta = \left(\frac{W_0 - W}{W_0}\right) \quad \ldots (3)$$

We define "W" and "W_0" as the weight losses experienced by Mild Steel samples (mg) with and without inhibitor.

Electrochemical studies

Potentiodynamic Polarization Study (PPS)

The electrochemical investigations were performed by utilizing a three-electrode assemblage and the CHI-66 model potentiostat. As the working electrode, mild steel specimens of 1 cm^2 were used along with platinum foil and calomel electrodes as the reference electrode and counter electrode[18]. We measured the degree of polarization of the working electrode by exposing it to a solution for 30 min with and without PSPA. Automated polarization curves were generated by switching the electrode potential from -500 mV to +500 mV at a scanning rate of 1 mV S^{-1} (Ref.19). We determined corrosion current density (I_{corr}) values as a function of Tafel intersections. The efficacy of the inhibitor was measured with the following Eq (4).

$$IE(\%) = \left[\frac{i_{corr} - i_{corr\ (inh)}}{i_{corr}}\right] X\ 100 \quad \ldots (4)$$

Corrosion current densities are denoted by $I_{corr(inh)}$ and I_{corr} in the 1M HCl solution.

Impedance Study

We investigated electrochemical impedance within the frequency range of 100 kHz to 10 MHz by using AC signals at the open circuit potential and the maximum amplitude of 5 mV. A Nyquist plot measuring the starting and stopping positions of different inhibitor concentrations was used to determine the investigatory charge transfer resistance (R_{ct})[20]. Based on the charge transfer resistance data, electrical double-layer capacities (C_{dl}) and inhibition efficiencies of the inhibitors were calculated using Eqs (5) and (5), respectively.

$$C_{dl} = \frac{1}{2\pi . f_{max} . R_{ct}} \quad \ldots (5)$$

$$IE(\%) = \left[\frac{R_{ct\ (inh)} - R_{ct}}{R_{ct}}\right] X\ 100 \quad \ldots (6)$$

In this equation, f_{max} is the peak frequency of the Nyquist plots, and $R_{ct(inh)}$ and R_{ct} are the resistances to charge transfer with and without the inhibitor.

Morphological Investigation

To analyze corrosion products on metal surfaces, scanning electron microscopy (SEM), energy-dispersive X-ray spectroscopy (EDS), and atomic force microscopy (AFM) were used[21,22]. These findings highlighted some intriguing concerns about the expediency of PSPA in preventing Mild steel specimen deterioration in corrosive conditions.

Theoretical Study

Theoretical considerations of PSPA's reactivity was carried out utilizing DFT and Natural Population Analysis (NPA) with Gaussian 09W software ["B3LYP/6-31G (d, p) basis set"] [23].

Results and Discussion

Mass reduction technique

As seen in Fig. 1, the rate of corrosion and the effectiveness of the suppression were correlated by the mass loss method in the 1M HCl solution at room temperature. It demonstrates unequivocally that as

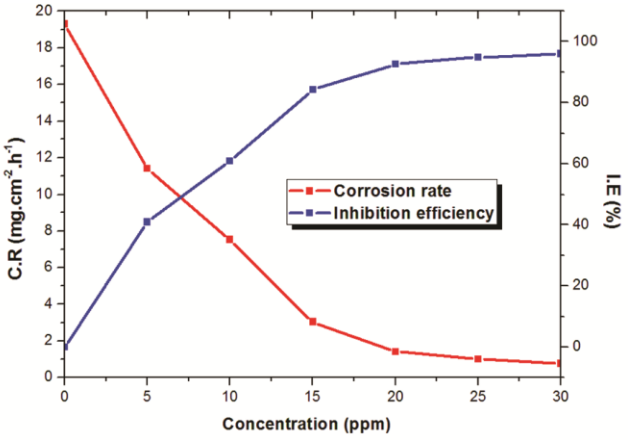

Fig. 1 — Relationship between the rate of corrosion and hindered efficacy of PSPA on Mild steel corrosion

inhibitor concentration increases, inhibition ability rises linearly while the corrosion rate decreases.

Table 2 includes more statistics on corrosion, including corrosion rate, effectiveness of the inhibition, and surface coverage. It shows that when PSPA concentration increases, the weight loss of the specimen slows and the rate of deterioration decreases in parallel. Additionally, the PSPA is more effective at protecting metallic surfaces from corrosion, as evidenced by the rising surface coverage values [24].

Electrochemical Polarization Technique

The Tafel lines for the test specimens in the 1M HCl medium at room temperature are shown in Fig. 2 in both the absence and presence of various PSPA concentrations. Tafel lines can be seen on anodic and cathodic sites, showing that PSPA prevents mild steel from oxidizing or reducing in an acidic environment. The obtained polarization parameters displayed in Table 2 supports the earlier assertion. As a general rule, E_{corr} values differ by more than ± 85 mV between an inhibitor and a blank, indicating that the inhibitor is either cathode or anode-based[25]. This polarization analysis shows the examined PSPA is a mixed-type protector, as indicated by its E_{corr} values within ± 85 mV. As evidenced by the Tafel slope values b_c and b_a provided in Table 3, the Tafel effect is seen on both the anode and cathode, with greater values of b_c showing cathodic preponderance. As PSPA concentrations increase, I_{corr} values decrease, indicating that PSPA molecules suppress corrosion current, and the observed efficiency is 95.13% at 30 ppm.

Table 2 — Mild steel corrosion factors of PSPA

C (ppm)	C.R (mg $cm^{-2}h^{-1}$)	I.E (%)	θ
Blank	19.3028	-	-
5	11.4098	40.89	0.41
10	7.5336	60.97	0.61
15	3.0336	84.28	0.84
20	1.4128	92.68	0.93
25	0.9985	94.83	0.95
30	0.7615	96.06	0.96

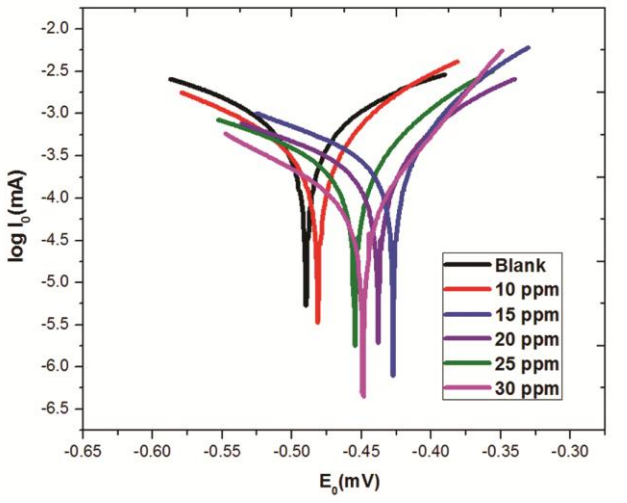

Fig. 2 — Polarization curves for different PSPA concentrations on mild steel corrosion

Electrochemical Impedance Technique

According to Fig. 3, the addition of PSPA enhances the hindrance of charge transfer because the diameter of Nyquist plots increases when PSPA concentration in the 1M HCl solution increases. Moreover, Table 3 provides a summary of the impedance factors, including charge transfer resistance (R_{ct}), electrical double-layer capacitance (C_{dl}), and hindrance efficacy (IE).

From Table 3, we can see clearly that the addition of PSPA significantly slows the electrochemical corrosion process as evidenced by the increasing values of R_{ct}, and the stalling process is also confirmed by the decreasing values of C_{dl}[26]. The highest efficiency of this approach is 95.51 % at 30 ppm, confirming that the PSPA is a competent protector in 1M HCl solution. Therefore, the examined PSPA protector has the significant potential to suppress the deterioration according to the electrochemical investigation.

Temperature Effect

The mass loss experiment in 1M HCl at different temperatures (304, 314, 324, and 334 K) demonstrated a correlation between preventive performance and temperature, as shown in Fig. 4. Table 4 provides a summary of the rate of deterioration and efficacy data at various PSPA concentrations. It is noticeable that, as a function of temperature, the inhibitory effectiveness diminishes with increasing protector concentration due to enhanced kinetic energy causing more forceful molecular collisions, disrupting the protective layer. Higher temperatures reduce adsorption and may induce thermal degradation of inhibitor molecules, diminishing their effectiveness. Competitive adsorption at increased concentrations leads to inefficient surface coverage. Furthermore, elevated temperatures facilitate oxygen transport to the metal surface, promoting oxidation and reducing inhibition[27]. We conclude from the tabulated results that the protective ability of PSPA decreases at increased temperatures for all the concentrations

Table 3 — Electrochemical polarization factors for PSPA on mild steel corrosion

Sample	Polarization parameters					Impedance parameters		
C (ppm)	E_{corr} (mV)	I_{corr} (mA)	b_c (mV)	b_a (mV)	IE (%)	R_{ct} (Ω cm^2)	C_{dl} (μF cm^{-2})	I.E (%)
blank	-487.67	1.893	372.29	311.05	0	1061.25	0.516	0
10	-481.34	0.752	186.64	104.40	60.25	2702.55	0.299	60.73
15	-427.26	0.312	466.91	117.16	83.51	6674.58	0.076	84.10
20	-438.14	0.146	303.11	258.34	92.28	13044.23	0.013	91.86
25	-454.87	0.112	252.84	112.68	94.07	19159.97	0.0056	94.46
30	-451.64	0.092	268.63	98.06	95.13	23634.84	0.0043	95.51

Table 4 — Relationship between rate of corrosion and hindered efficacy for PSPA on Mild steel corrosion

C (ppm)	C.R (mg cm^{-2} h^{-1})				I.E (%)			
	304K	314K	324K	334K	304K	314K	324K	334K
Blank	19.3	20.88	31.41	46.1	0	0	0	0
5	11.41	14.15	26.89	42.39	40.89	32.23	14.4	8.05
10	7.53	10.48	22.71	38.78	60.97	49.81	27.7	15.89
15	3.03	5.03	15.07	27.91	84.28	75.92	52.02	39.46
20	1.41	3.94	8.78	15.69	92.68	81.14	72.05	65.98
25	1	2.41	6.33	12.04	94.83	88.47	79.86	73.9
30	0.76	2.03	5.38	10.94	96.06	90.29	82.86	76.28

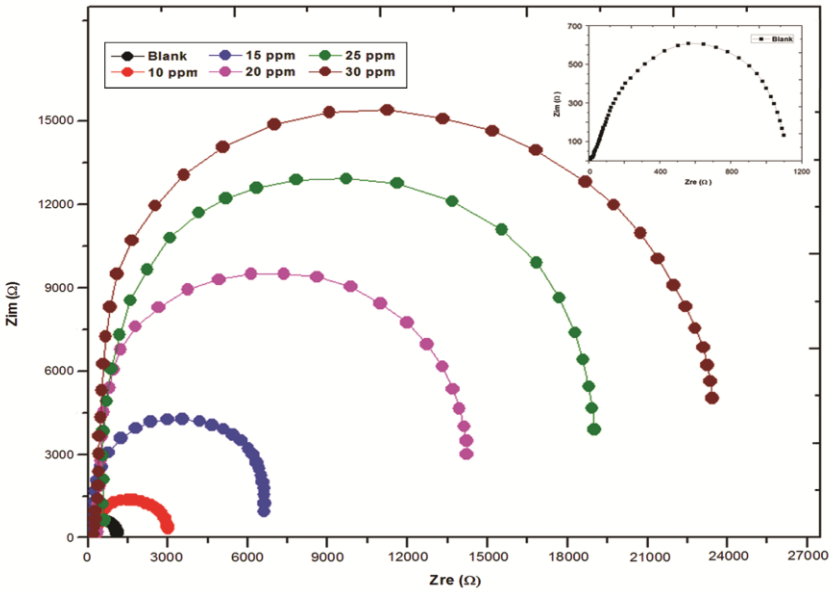

Fig. 3 — Nyquist plots for different concentrations of PSPA on Mild corrosion

implying that the adsorption mechanism is physisorption.

Corrosion Kinetics and Adsorption Thermodynamics

The temperature study was employed to apply the Arrhenius equation (Eq. 7) to derive the kinetic parameters at various temperatures, including the activation energy (E_a) and the Arrhenius factor (A).

$$\log CR = \log A - \frac{Ea}{RT} \quad \ldots (7)$$

The activation energy and Arrhenius factor at various temperatures were attained using the Eq. (7). With a slope of ($-E_a/2.303R$) and an intercept of (log A), the Arrhenius plots obtained by graphing (log CR) against ("1000/T") are shown in Fig. 5a. The slope and intercept of the straight lines were taken to determine the E_a and A values, respectively.

Table 3 shows that E_a values ascended when PSPA concentration increased. It demonstrated that the energy barrier rises during the corrosion inhibition process at higher temperatures. Physical adsorption is mentioned as the adsorption process, and rising Arrhenius factor values are used to support this claim[28, 29].

Furthermore, ΔH^0 and ΔS^0 values were obtained by plotting "log CR/T" versus "1000/T" with slope "$(-\Delta H^0/2.303R)$" and intercept "[(log (R/Nh) + $\Delta S^0/2.303R$)" using transition state Eq. (8).

$$\log\left(\frac{CR}{T}\right) = \log\left(\frac{RT}{Nh}\right) + \left(\frac{\Delta S^0}{2.303R}\right) - \left(\frac{\Delta H^0}{2.303RT}\right) \quad \ldots (8)$$

The transition state illustrations for different concentrations of PSPA on mild steel in the 1 M HCl solution are shown in Fig. 5b. Straight lines are achieved by the relationship of "log CR/T" against "1000/T" with slope "$(-\Delta H^0/2.303R)$" and intercept "[(log (R/Nh) + $\Delta S^0/2.303R$]". Additionally, ΔH^0 and ΔS^0 values were determined using the slope and intercept of the transition state lines, and they are shown in Table 5 along with other relevant information.

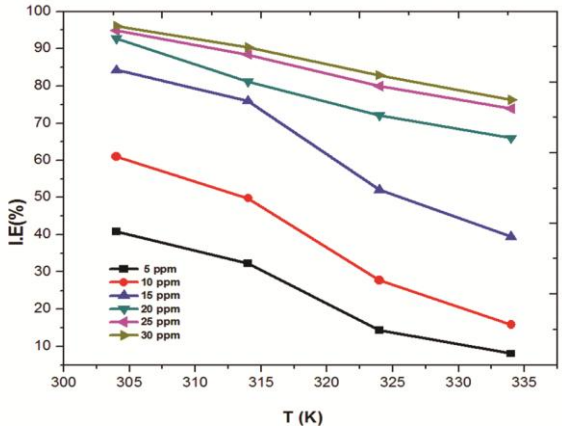

Fig. 4 — Relationship between the temperatures and hindered efficacy of PSPA on mild steel corrosion

Negative values of S^0 changed to positive track indicating that the adsorption process's uncertainty increases from blank to 30 ppm in an acidic environment and positive ΔH^0 values represent the endothermic adsorption[30]. Furthermore, the average E_a-ΔH^0 value (2.65 kJ mol^{-1}) is substantially comparable to the RT value (2.61 kJ mol^{-1}) demonstrating that the thermodynamic activation factors affect the corrosion adsorption inhibition.

Freundlich Adsorption Isotherm

The number of adsorption isotherm models identifies the adsorption capabilities of the inhibitory mechanism. The Freundlich isotherm is the model that fits this situation the best, and Eq. (9) is used for obtaining the adsorption parameters.

$$\log\theta = \log K + \frac{1}{n}\log C \quad \ldots (9)$$

As illustrated in Fig. 6, the Freundlich equation was used to display "(log) vs (log C)," and the adsorption

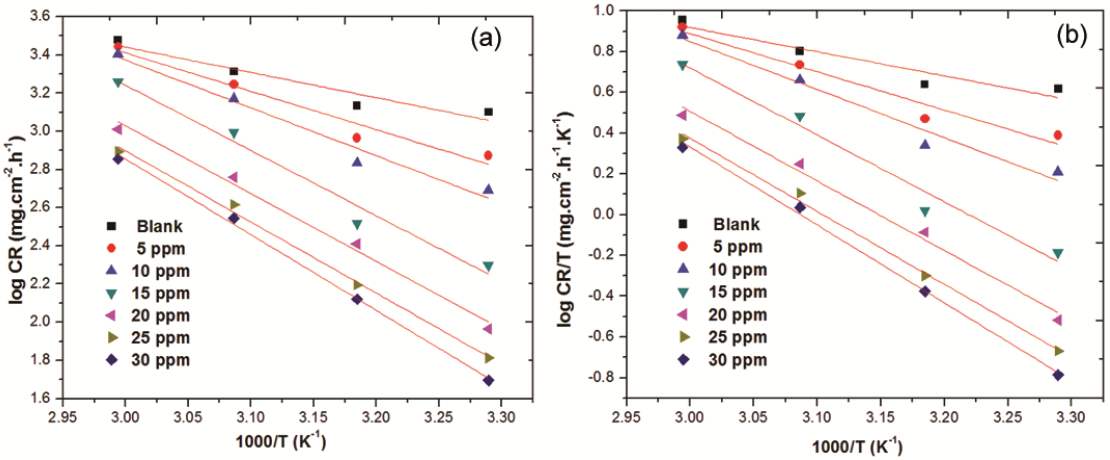

Fig. 5 — (a) Arrhenius and (b) transition state lines for PSPA on mild steel corrosion at different temperatures

Table 5 — Kinetic and Thermodynamic factors of PSPA on mild steel corrosion

C (ppm)	E_a (KJ mol^{-1})	A	ΔH^0 (KJ mol^{-1})	ΔS^0 (JK^{-1} mol^{-1})	E_a- ΔH^0
blank	25.32	2.5603 X 10^8	22.68	-111.97	2.65
5	38.51	2.7854 X 10^{10}	35.86	-72.98	2.65
10	47.89	7.5335 X 10^{11}	45.24	-45.56	2.65
15	65.38	3.0549 X 10^{13}	62.74	4.37	2.65
20	67.94	4.7097 X 10^{13}	65.29	7.97	2.65
25	71.30	1.1695 X 10^{14}	68.65	15.53	2.65
30	75.84	5.4450 X 10^{14}	73.19	28.34	2.65

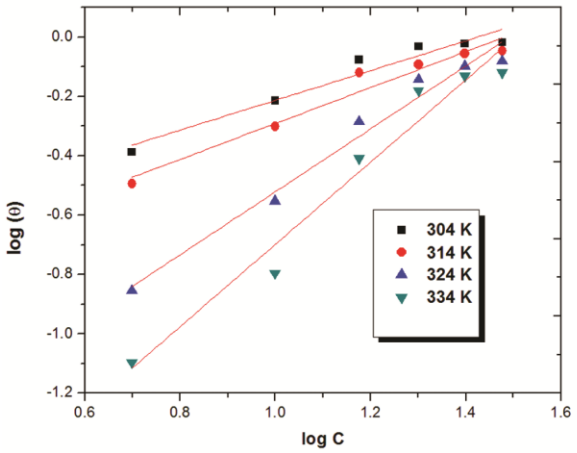

Fig. 6 — Freundlich isotherm for PSPA on Mild steel corrosion at different temperatures

factors "K_{ads}" and "n" were obtained from the "slope" and "intercept" of the straight lines, respectively.

Moreover, using Eq. (10), the adsorption standard free energy values (ΔG^0 ads) were calculated and are shown in Table 6.

$$\Delta G_{ads} = [-RT \ln(55.5\ K_{ads})] \quad \ldots (10)$$

Table 6 shows that as the temperature rises, decreasing K_{ads} values imply physical adsorption and decreasing 'n' values disclose desorption during the corrosion inhibition process in 1M HCl solution[31]. Furthermore, the negative ΔG^0 values demonstrate that the adsorption process is spontaneous and physisorption for all worked concentrations of PSPA in an acidic corrosive environment at elevated temperatures.

Table 6 — Freundlich data of PSPA on Mild steel corrosion at various temperatures

T (K)	Freundlich parameters			
	K_{ads}	ΔG^0 (KJmol^{-1})	n	R^2
304	19.320	-17.64	1.99	0.9331
314	12.735	-17.13	1.65	0.9444
324	2.624	-13.42	0.94	0.9697
334	0.826	-10.62	0.72	0.955

Theoretical Investigation

DFT Investigation

The optimized structure, ESP map, E_{HOMO}, and E_{LUMO} of the explored PSPA are shown in Figs 7a, 7b, 7c & 7d, respectively. The FMO theory states that the energy value of the HOMO demonstrates the capability of transferring electrons to the acceptor, while the energy value of the LUMO demonstrates the inhibitor's capacity to receive electrons from the metal via back donation[32]. As we seen in Fig. 7c, HOMO focuses on almost every portion of the inhibitor molecule indicating that those locations are the coordination sites for strong inhibition causing chemisorption. Conversely, LUMO focuses primarily on the N atom of the piperidine ring, the SO_2 group, and the benzene ring, all of which are the focal point for accepting electrons from the metal to inhibitor retro donation, resulting in chemisorption as shown in Fig. 7d.

These suggestions are furthermore corroborated by the inspection of the ESP map of the inspected molecule which is seen in Fig. 7b. ESP map reflects the electronic potential of the constituents of the PSPA. In general Red reflected areas show the electron donating centers and blue shaded parts mention the electron receiving sites of the inhibitor[33]. Herein, the red clouds cover predominantly SO_2, and –C=O groups which confirm the electrons transfer from these groups to mild steel whereas the blue sites on the piperidine ring act as a receiving part of the molecule.

Additionally, Mulliken charges of the electronegative atoms in the molecule revealing that the coordination sites and protonation center of the inhibitor. The lower negative value of O_{12} (-0.173) implies that it has a higher proclivity for protonation and can easily interact with negatively charged steel surfaces via physisorption. Due to their lower negative values, the other mentioned atoms imply that electrons migrate from these locations to the iron's unoccupied d orbital for coordination through chemisorption [34].

Furthermore, the additional important electronic properties ΔE, D, I, A, χ, η, σ and ΔN were acquired from the frontier molecular orbital energies by the following Eqs (11-17)

$$\Delta E = E_{HOMO} - E_{LUMO} \quad \ldots (11)$$

$$I = -E_{HOMO} \quad \ldots (12)$$

$$A = -E_{LUMO} \quad \ldots (13)$$

$$\chi = -\frac{1}{2}(E_{LUMO} + E_{HOMO}) \quad \ldots (14)$$

$$\eta = -\frac{1}{2}(E_{HOMO} - E_{LUMO}) \quad \ldots (15)$$

$$\sigma = \frac{1}{\eta} \quad \ldots (16)$$

$$\Delta N = \frac{\phi - \chi_{inh}}{[2(\eta_{Fe} + \eta_{inh})]} \quad \ldots (17)$$

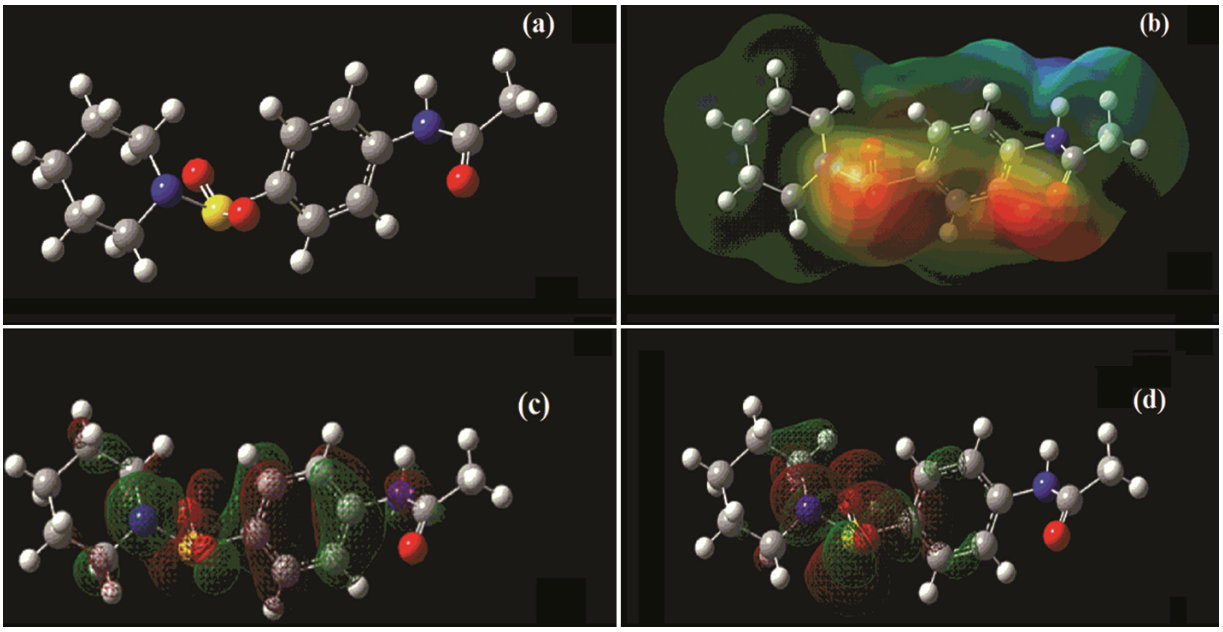

Fig. 7 — Optimized structure (b) ESP map (c) E_{HOMO} (d) E_{LUMO} distribution of PSPA

Table 7 — Electronic parameters of the PSPA molecule

Electronic parameters	
E_{HOMO}	-5.523 (eV)
E_{LUMO}	-0.8629 (eV)
Energy Gap (ΔE)	4.66 (eV)
Dipolemoment (D)	4.3
Ionization energy (I)	5.5229 (eV)
Electron affinity (A)	0.8628 (eV)
Absolute electronegativity (χ)	3.1929(eV)
Global hardness (η)	2.3300
Global softness (σ)	0.4291
Transferred electron fraction (ΔN)	0.3491
Back donation ($\Delta_{Eback\ donation}$)	-0.5825 (eV)

Higher negative values of HOMO often suggest a better propensity to donate electrons, whereas lower negative values of LUMO typically designate a greater tendency to receive electrons by retro-donation.

As we seen from Table 7, E_{HOMO} (-5.523 eV) implies that electrons can be donated from the inhibitor to the Mild steel whereas E_{LUMO} (-0.8629 eV) suggests that electrons may be donated from the metal to the inhibitor. The reactivity of PSPA is represented by other factors such as ΔE, D, I, A, χ, η, σ, and ΔN. Altogether, the data revealed that PSPA has a high prospect of mitigating corrosion in an acidic environment.

Fukui Indices

The key analysis to forecast the inhibitor's local reactivity gives a chemical understanding of the inhibition process through the use of condensed Fukui functions. As we can see, every atom has a notable propensity to take and donate electrons necessary for the inhibition process. Electrophilic and nucleophilic condensed Fukui functions were constructed from the following equations.

$$F_k^+ = P_k(N+1) - P_K(N) \quad \ldots (18)$$

$$F_k^- = P_k(N) - P_K(N-1) \quad \ldots (19)$$

$$F_k^0 = P_k(N+1) - P_K(N-1) \quad \ldots (20)$$

WhereF_k^-, F_k^+ and F_k^0 represent the 'Natural populations" of the element K in the anionic, cationic, and neutral atoms, respectively. The electrophilic and nucleophilic sites of PSPA are displayed in Table 8 by the computed condensed Fukui functions. The larger value F_k^+, corresponds to the nucleophilic reactivity of the inhibition process, whereas the larger value F_k^- corresponds to the electrophilic reactivity [35]. From Table 8, we can infer that the nucleophilic sites S_{11} (1.975), N_{14} (0.203), and O_{13} (0.104) are the electron donation centers for mild steel, whereas the electrophilic sites C_6 (0.759), C_2 (0.178), and C_4 (0.15) are the most electrophilic reactive sites. The areas where the electrophilic attack is directed are those in which the metal is most likely to release electrons via back donation to form a coordinating bond.

Surface Characterisation

SEM

Figs 8a–8d displays SEM micrographs of bare Mild steel, unshielded, and shielded metallic surfaces

Table 8 — Fukui indices for PSPA

PSPA	N-1	N	N+1	F_k^-	F_k^+
C1	0.62	-0.182	-0.179	-0.802	0.003
C2	-0.422	-0.244	-0.199	**0.178**	0.045
C3	0.087	0.134	0.17	0.047	0.036
C4	-0.381	-0.231	-0.219	**0.15**	0.012
C5	0.471	-0.218	0.198	-0.689	**0.416**
C6	-1.067	-0.308	-0.294	**0.759**	0.014
H7	0.237	0.263	0.279	0.026	0.016
H8	0.292	0.301	0.314	0.009	0.013
H9	0.225	0.251	0.271	0.026	0.02
H10	0.42	0.247	0.246	-0.173	-0.001
S11	2.349	0.301	2.276	-2.048	**1.975**
O12	-0.975	-0.941	-0.88	0.034	0.061
O13	-1.006	-0.971	-0.867	0.035	**0.104**
N14	-0.73	-0.715	-0.512	0.015	**0.203**
C15	-0.264	-0.263	-0.274	0.001	-0.011
H16	0.222	0.235	0.268	0.013	0.033
H17	0.247	0.256	0.285	0.009	0.029
C18	-0.269	-0.263	-0.272	0.006	-0.009
H19	0.22	0.236	0.268	0.016	0.032
H20	0.223	0.222	0.245	-0.001	0.023
C21	-0.487	-0.485	-0.46	0.002	0.025
H22	0.211	0.226	0.262	0.015	0.036
H23	0.273	0.271	0.28	-0.002	0.009
C24	-0.487	-0.486	-0.462	0.001	0.024
H25	0.209	0.223	0.257	0.014	0.034
H26	0.273	0.268	0.275	-0.005	0.007
C27	-0.443	-0.445	-0.449	-0.002	-0.004
H28	0.224	0.234	0.277	0.01	0.043
H29	0.2	0.211	0.238	0.011	0.027
N30	-0.753	-0.733	-0.685	0.02	0.048
H31	0.384	0.428	0.443	0.044	0.015
O32	0.681	-0.582	-0.523	-1.263	0.059
C33	0.597	0.722	0.737	0.125	0.015
C34	-0.72	-0.735	-0.731	-0.015	0.004
H35	0.235	0.263	0.277	0.028	0.014
H36	0.227	0.249	0.262	0.022	0.013
H37	0.158	0.255	0.273	0.097	0.018

of PSPA in 1M HCl solution. The specimen has a smoother surface with a few light scrapes before immersion in the corrosive solution, as shown in Fig. 8a. In the absence of PSPA, rust formation leads to a severely damaged surface, as seen in Fig. 8b. Furthermore, Figs 8c & 8d at 30 ppm show the smooth surface with the protective mass when PSPA is present. These SEM images assist us to establish that the tested PSPA operated well in the challenging environment, proving that the development of a thin coat on the metallic surface in 1M HCl solution inhibits corrosion.

EDS

Figs 9a–9c depict the EDS interpretation of polished steel, unshielded steels, and shielded steels with PSPA in 1M HCl at ambient temperature. The representation in Fig. 9a makes it evident that the main constituents present in polished mild steel are C, O, N, and Fe. The formation of a chlorine peak without PSPA, combined with the examined components shown in Fig. 9b, demonstrates the severely corroded steel surface. Fig. 9c shows that the nitrogen peak advent indicates the presence of PSPA, which shields the steel surface by transferring electrons from the "N" and "O" atoms to the Fe atom, demonstrating a chemical connection. Additionally, the quantitative data from the EDS investigation, also supports corrosion prevention. N (1.65%) and O (36.27%) weight percentages show that the formation of a coordinating bond with PSPA and mild steel in the presence of 1M HCl effectively inhibits the active sites of metallic surfaces.

AFM

Figs 10a–10c depict the AFM patterns of the bare, unshielded, and shielded with PSPA at 30 ppm, respectively. The bare steel surface exhibits a regular surface with tiny pits as shown in Fig. 10a; nonetheless, the unprotected metallic surface exposes a comparatively uneven and porous framework with deep pores in the presence of a corrosive environment. The inhibited surface is overall smoother than the specimen submerged in the corrosive solution indicating that PSPA causes the roughness to reduce as shown in Fig. 10c.

Additionally, the average roughness measurements of the steel specimens before dipping, unshielded, and shielded surfaces in acidic corrosive environments are 279.41 nm, 418.32 nm, and 290.63 nm, respectively, and the corresponding RMS values are 332.27 nm, 489.49 nm, and 364.81 nm, implying the surface protection. In this study, it is observed that the PSPA protector significantly reduces the similarity of the observed roughness data between the protected surfaces and bare steel surfaces. As the mild steel surface has been encapsulated with an impenetrable and organized barrier, all AFM data indicate that the surface is smooth.

Inhibition mechanism

Several variables, such as the electronic structure, molecule size, shape, charge on the metal surface, etc., affect how well PSPA prevents the deterioration of mild steel in the 1M HCl solution. The inhibition

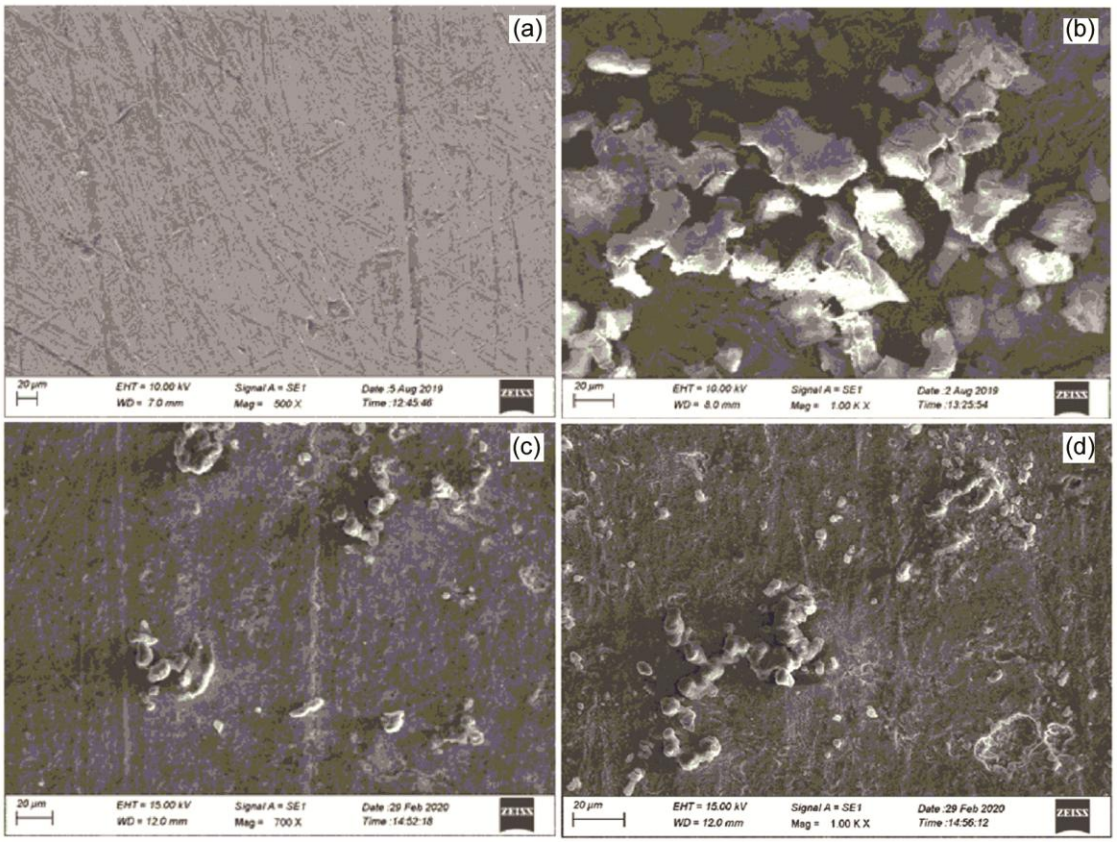

Fig. 8 — SEM micrographs for (a) polished surface (b) unshielded and, (c) & (d) shielded surfaces with PSPA

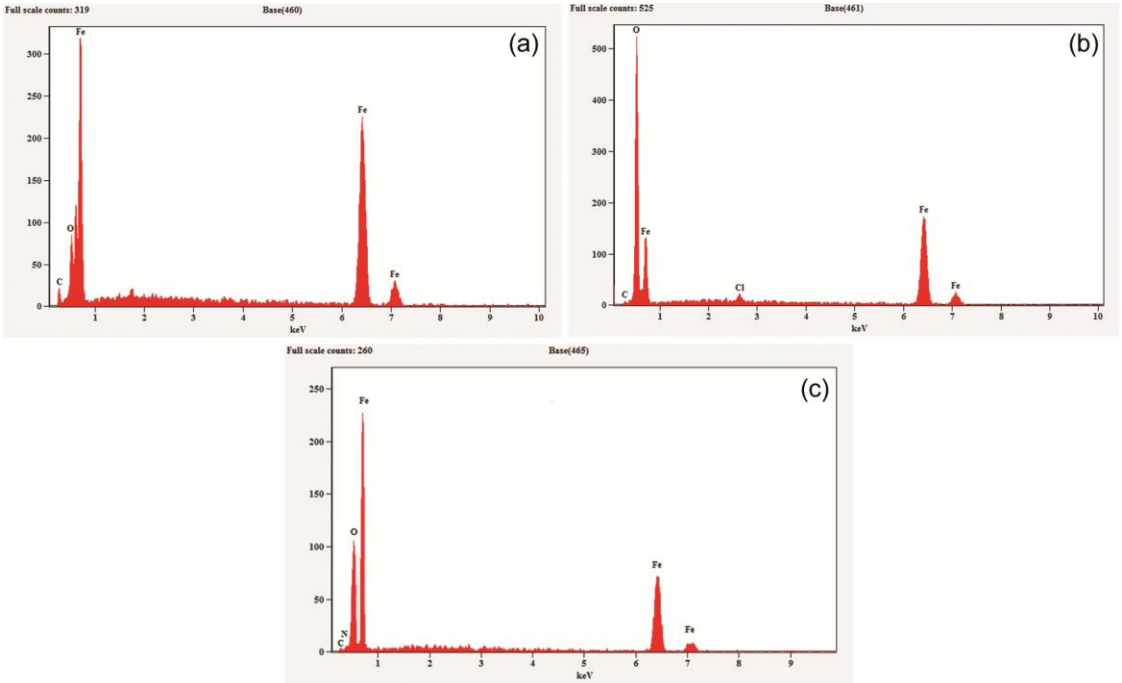

Fig. 9 — EDS spectra of (a) polished surface (b) unshielded and (c) shielded surface with PSPA

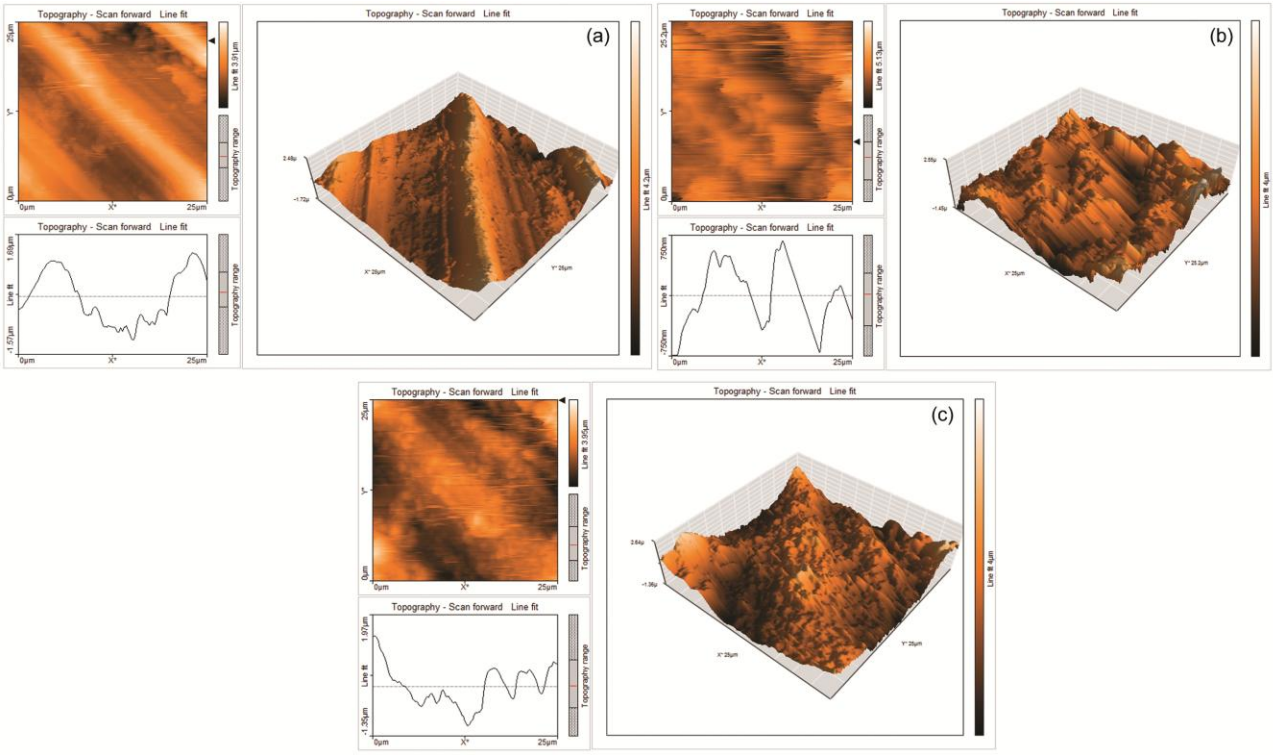

Fig. 10 — AFM pattern of (a) plain surface, (b) unshielded and, (c) shielded surfaces with PSPA

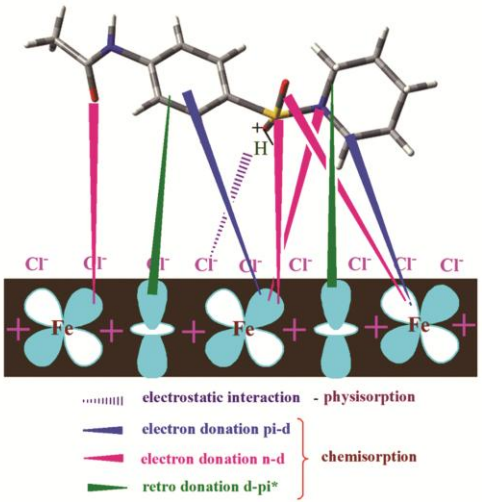

Fig. 11 — Schematic representation of PSPA adsorption modes with the steel surface in 1M HCl solution

process may entail physisorption, chemisorption, or a combination of the two depending on the aforementioned criteria. The adsorption process is physisorption, which was further verified by kinetic, thermodynamic, and isothermal experiments. Also, the chemisorption process is supported by computation-based assessments of the HOMO, LUMO charge distribution, and the NBO charge populations. Based on theoretical and experimental results, Fig. 11 displays a schematic portrayal of multiple PSPA adsorption modes on the surface of the mild steel.

Conclusion

The anti-corrosive effect of N-(4-(piperidin-1-ylsulfonyl) phenyl) acetamide (PSPA) on mild steel corrosion was successfully analyzed utilizing mass loss, potentiodynamic polarization, impedance analysis, temperature study, surface examination, and quantum chemical study. A good degree of agreement exists between the inhibitory performance as determined by mass loss, potentiodynamic, and impedance studies. Furthermore, the results of the potentiodynamic results demonstrated that PSPA acted as a mixed-type protector, preventing the evolution of cathodic hydrogen gas as well as the dissolution of anodic metal. Additionally, impedance inquiry exposed that the R_{ct} ability increased with rising PSPA concentration and that the inhibitory process was supported by lowering electrical double-layer capacitance values. Adsorption was electrostatically occurring because the energy barrier increased with concentration and the adsorption process obeyed the Freundlich isotherm, according to activation parameters. The high degree of efficiency achieved through chemical adsorption

was supported by all quantum chemical parameters. The Fukui condensed function revealed an immense amount of information regarding inhibitory mechanisms. SEM, EDS, and AFM surface analyses validated the PSPA's mild steel corrosion mitigation behaviour. In conclusion, all of the aforementioned shreds of evidence supported the claim that the tested PSPA is highly effective in preventing the deterioration of mild steel in 1M HCl solution.

References

1 Kadhim A, Al-Okbi A K, Jamil D M, Qussay A, Al-Amiery A A & Gaaz T S, Experimental and theoretical studies of benzoxazines corrosion inhibitors, *Results Phys*, 7 (2017) 4013.

2 Yıldız R, Adsorption and inhibition effect of 2, 4-diamino-6-hydroxypyrimidine for mild steel corrosion in HCl medium: Experimental and theoretical investigation, *Ionics*, 25 *(*2019) 859.

3 Resen A M, Hanoon M, Salim R D, Al-Amiery A A, Shaker L M & Kadhum A A H, Gravimetrical, theoretical, and surface morphological investigations of corrosion inhibition effect of 4-(benzoimidazole-2-yl) pyridine on mild steel in hydrochloric acid, *Koroze a Ochrana Materialu*, 64 (2020) 122.

4 Masoumi A, Hossaini-Sadr M & Soltani B, Pyrazole ligands and their monometallic and bimetallic complexes: Synthesis, characterization, and application as novel corrosion inhibitors, *J Adhes Sci Technol*, 34 (2020) 2569.

5 Fu J, Li S, Wang Y, Cao L & Lu L, Computational and electrochemical studies of some amino acid compounds as corrosion inhibitors for mild steel in hydrochloric acid solution, *J Mater Sci*, 45 (2010) 6255.

6 Al-Baghdadi S B, Hashim F G, Salam A Q, Abed T K, Gaaz T S & Al-Amiery A A, Synthesis and corrosion inhibition application of NATN on mild steel surface in acidic media complemented with DFT studies, *Results Phys*, 8 (2018) 1178.

7 Erteeb M A, *Sci Technol*, 8 (2020) 16. Please provide the title of this reference

8 Ibrahim M A A, Moussa N A M, Mahmoud A H M, Sayed S R M, Sidhom P A & Abd-El-Rahman M K, Density functional theory study of the corrosion inhibition performance of 6-mercaptopurine and 6-thioguanine expired drugs toward the aluminium (111) surface, *RSC Adv*, 13 (2023) 29023.

9 Beda R H B, Niamien P M, Avo-Bilé E B & Trokourey A, Inhibition of aluminium corrosion in 1.0 M HCl by caffeine: Experimental and DFT studies, *Adv Chem*, 2017 (2017) 6975248.

10 Lgaz H, Salghi R, Chaouiki A, Shubhalaxmi, Jodeh S & Bhat K S, Pyrazoline derivatives as possible corrosion inhibitors for mild steel in acidic media: A combined experimental and theoretical approach, *Cogent Eng*, 5 (2018) 1441585.

11 Kaya S, Guo L, Kaya C, Tüzün B, Obot I B & Touir R, Quantum chemical and molecular dynamic simulation studies for the prediction of inhibition efficiencies of some piperidine derivatives on the corrosion of iron, *J Taiwan Inst Chem Eng*, 65 (2016) 522.

12 Jeeva M, Venkatesa P G & Rajesh C M, Inhibition effect of nicotinamide and its Mannich base derivatives on mild steel corrosion in HCl, *J Mater Sci*, 52 (2017) 12861.

13 Rajendraprasad S, Ali S & Prasanna B M, Electrochemical behavior of N^1-(3-methylphenyl)piperidine-1,4-dicarboxamide as a corrosion inhibitor for soft-cast steel carbon steel in 1 M HCl, *J Fail Anal Preven*, 20 (2020) 235.

14 Ilies M A, Vullo D, Pastorek J, Scozzafava A, Ilies M & Caproiu M T, Carbonic anhydrase inhibitors inhibition of tumor-associated isozyme IX by halogenosulfanilamide and halogenophenylaminobenzolamide derivatives, *J Med Chem*, 46 (2003) 2187.

15 De-Castro-Barbosa M L, De-Albuquerque-Melo G M, Da-Silva Y K C, De-Oliveira-Lopes R, De-Souza E T & De-Queiroz A C, Synthesis and pharmacological evaluation of N-phenyl-acetamide sulfonamides designed as novel non-hepatotoxic analgesic candidates, *Eur J Med Chem*, 44 (2009) 3612.

16 Tribak Z, Skalli M K, Haoudi A, Rodi Y K & Senhaji O, Comparative studies on the corrosion inhibition of three different organic heterocyclic compounds as corrosion inhibitors for mild steel in hydrochloric acid, *J Mex Chem Soc*, 64 (2020) 1247.

17 Husaini M & Ibrahim M B, Investigation of inhibition potential effect of organic compound for the corrosivity of phosphoric acid on aluminium, *Int J Eng Manuf*, 10 (2020) 41.

18 Vijayalakshmi K & Elangovan J, 1,2,3-Triazole derivative as a potential protector for mild steel corrosion in acid media: A kinetic and thermodynamic approach, *J Indian Chem Soc*, 97 (2020) 1574.

19 Draoui Y, Radi S, Tanan A, Oulmidi A, Miras H N & Benabbes R, Novel family of bis-pyrazole coordination complexes as potent antibacterial and antifungal agents, *RSC Adv*, 12 (2022) 17755.

20 González-Olvera R, Román-Rodríguez V, Negrón-Silva G, Espinoza-Vázquez A, Rodríguez-Gómez F & Santillan R, Multicomponent synthesis and evaluation of new 1,2,3-triazole derivatives of dihydropyrimidinones as acidic corrosion inhibitors for steel, *Molecules*, 21 (2016) 250.

21 Ganapathi Sundaram R & Sundaravadivelu M, *J Metall*, 9 (2016) 1.Please provide the title of this reference

22 Haque J, Verma C, Srivastava V, Quraishi M A & Ebenso E E, Experimental and quantum chemical studies of functionalized tetrahydropyridines as corrosion inhibitors for mild steel in 1 M hydrochloric acid, *Results Phys*, 9 (2018) 1481.

23 Singh A, Ansari K R, Haque J, Dohare P, Lgaz H & Salghi R, Effect of electron donating functional groups on corrosion inhibition of mild steel in hydrochloric acid: Experimental and quantum chemical study, *J Taiwan Inst Chem Eng*, 82 (2018) 233.

24 Vijayalakshmi K, Punitha N, Rengasamy R & Elangovan J, Effect of 1, 2, 3-triazole derivative on the dissolution performance of mild steel in 1M HCl medium, *Indian J Chem Technol*, 28 (2021) 421.

25 Espinoza-Vázquez A, Rodríguez-Gómez F J, Martínez-Cruz I K, Ángeles-Beltrán D, Negrón-Silva G E & Palomar-Pardavé M, Adsorption and corrosion inhibition behaviour of new theophylline-triazole-based derivatives for steel in acidic medium, *Royal Soc Open Sci*, 6 (2019) 181738.

26 Motawea M M, Electrochemical behavior and theoretical studies of arylazo (1-naphthyl-2-cyanoacetamide) derivatives as new corrosion inhibitors for Inconel 800 in chloride solution, *Sci Rep*, 14 (2024) 14683.
27 Nahlé A, Salim R, Hajjaji F E R, Aouad M, Messali M & Ech-chihbi E, Novel triazole derivatives as ecological corrosion inhibitors for mild steel in 1.0 M HCl: Experimental & theoretical approach, *RSC Adv*, 11 (2021) 4147.
28 Toghan A, Gadow H S, Fawzy A, Alhussain H & Salah H, Adsorption mechanism, kinetics, thermodynamics, and anticorrosion performance of a new thiophene derivative for C-steel in a 1.0 M HCl: Experimental and computational approaches, *Metals*, 13 (2023) 1565.
29 Chaudhary S, Tak R K, Kumari K & Sharma N, Thermodynamic and kinetic study of corrosion
30 inhibition of mild steel by plant extract in acidic medium, *Mater Int*, 6 (2024) 25.
31 Go L C, Depan D, Holmes W E, Gallo A, Knierim K & Bertrand T, Kinetic and thermodynamic analyses of the corrosion inhibition of synthetic extracellular polymeric substances, *Peer J Mater Sci*, 2 (2020) 24.
32 Ahmed S K, Ali W B & Khadom A A, Synthesis and investigations of heterocyclic compounds as corrosion inhibitors for mild steel in hydrochloric acid, *Int J Ind Chem*, 10 (2019) 159.
33 Raphael V P, Shanmughan S K & Kakkassery J T, *Int J Corros*, 16 (2016) 1. Please provide the title of this reference
34 Annon I A, Jlood K K, Hanoon M M, Sayyid F F, Al-Azzawi W K & Al-Amiery A, Corrosion inhibition of mild steel in HCl solution using MPO: Experimental and theoretical insights, *J Mater Eng*, 2 (2024) 104.
35 Dohare P, Quraishi M A, Verma C, Lgaz H, Salghi R & Ebenso E E, Ultrasound induced green synthesis of pyrazolo-pyridines as novel corrosion inhibitors useful for industrial pickling process: Experimental and theoretical approach, *Results Phys*, 13 (2019) 102344.
36 Hadisaputra S, Purwoko A A, Savalas L R T, Prasetyo N, Yuanita E, Hamdiani S, Quantum chemical and monte carlo simulation studies on inhibition performance of caffeine and its derivatives against corrosion of copper, *Coatings*, 10 (2020) 1086.